 CMES, vol.3, no.4, pp.431-446, 2002

Combining Lumped Parameter Bond Graphs with Finite Element Shafts in a Gearbox Model

J. Choi[1] **and M.D. Bryant**[2]

Abstract: This paper presents an updated bond graph model of a gearbox, which now includes bending of shafts. The gearbox system has an input shaft, layshaft, output shaft, spur gears, bearings, and housing. The bond graph model integrates separate sub-models into a composite model. Sub-modules include tooth-to-tooth contact, rotor dynamics of shafts, global dynamics of the gearbox housing structure, and shaft bending modeled by finite element modeling. The tooth-to-tooth model includes tooth bending; shaft torsion; gear inertia; conversion of gear torque into tooth forces; tooth contact mechanics; and multiple tooth contact. To analyze shaft dynamics more precisely, elementary finite element theory was adopted into the shaft bending module. The complete dynamics model was simulated, combining numerical methods for lumped elements and finite element techniques into a single code.

We will briefly review the gearbox bond graph model, present equations and numerical methods, explain simulation algorithms, and then present simulation results.

keyword: Gear, Gearbox, Bond graphs, Newmark's method, Finite element method (FEM).

1 Introduction

In this article, an existing model of a layshaft gearbox will be updated with bending of shafts. The gearbox system has input shaft, layshaft, output shaft, gears, bearings, gear tooth contacts, and gearbox housing. Our model employs bond graphs, an abstraction of the lumped parameter equivalent circuit analysis technique of electro-mechanics. Bond graphs can describe the dynamics of any physical system: mechanical, electrical, fluidic, thermodynamic, etc [Paynter (1960)]. Bond graphs map how and where power flows through, and energy is stored in, a physical system. Bond graphs are similar to circuit analysis techniques, applying Kirchoff like conservation laws to balance the physical effects of generalized sources, resistances, capacitances, inertances, transformers, and other elements. Bond graphs usually employ lumped parameter approximations. Bond graphs are also modular: an overall system model can be created by linking together models of individual components or sub-systems. State equations representative of the system dynamics can then be extracted from the bond graph for simulations [Karnopp, Margolis and Rosenberg (2000)].

Prior gear and gearbox models were piecemeal: these models examined certain facets of gear systems or gear tooth contacts separately [Özgüven and Houser (1988)]. Interactions were neglected. In this article, we have integrated whole gearbox physics into a composite model. Lumped parameter techniques – bond graphs – comprise most elements of this model. The model was augmented with finite elements, to account for multiple critical speeds of shafts. This presents special problems, combining the seemingly incompatible numerical methods of state equations with the second order matrix ordinary differential equations from FEM. This article formulates the aforementioned model, derives the mixed set of differential equations, generates a mixed numerical method for the gearbox system, and then presents solutions.

2 Layshaft gearbox model

An early bond graph model of a typical manual transmission layshaft gearbox for rear wheel drive vehicles was developed by Hrovat and Tobler [Hrovat and Tobler (1991)]. Utilizing a gear tooth contact sub-model [Kim and Bryant (1999)] and Hrovat and Tobler's bond graph model, a more detailed rotary model of a layshaft gearbox was assembled [Kim (1999)]. A schematic is presented in Fig. 1.

The system is composed of two pairs of gears, an input shaft, a layshaft, an output shaft, and a box which houses

[1] University of Texas, Austin, TX, U.S.A.
[2] University of Texas, Austin, TX, U.S.A

all gears and shafts. The box is mounted to the foundation with stiffness k_b and damping R_b. The angular velocities of input shaft, layshaft and output shaft are ω_i, ω_{23} and ω_o respectively. Each of gears is numbered and has a velocity ω_1, ω_2, ω_3, and ω_4. Due to the difference in torque on input and output shafts, the box can rotate around axis A-A′ with velocity ω_β. Relative velocities with respect to a coordinate frame attached to the box, and reaction forces acting on bearings attached to the box, are also shown in Fig. 1. Because the bearings are attached to the box, these reaction forces will be applied to the box and will generate torques on the box.

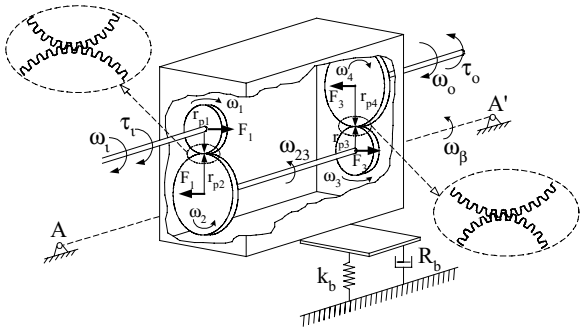

Figure 1 : Typical manual transmission layshaft gearbox [Hrovat and Tobler (1991)]

Fig. 2 contains a bond graph model updated from Hrovat and Tobler [Hrovat and Tobler (1991)] of the overall system shown in Fig. 1. All Inertance (I) elements are rotational mass moments of inertia associated with shafts, gears, or the gearbox housing. Likewise, all compliances (C) are torsional springs, and all resistances (R) are losses from bearings, except for the resistance at the bottom center of the bond graph which represents box to foundation damping R_b. The resistance next to the source 'MSf' located on the far left represents the losses of the bearing that supports the input shaft. The adjacent 'C' element represents the torsional compliance of the input shaft, and the accompanying 'I' element represents the rotational mass moment of inertia of the input shaft and first gear. The dashed boxes include gear teeth contact sub-models (shown as ellipses) and resistances that model losses of layshaft bearings. The power bonds extending from the bottom 1-junction in the gearbox housing and foundation section that form the 'triangular structure', model the reaction torque applied to the box by the shaft, bearings, and gears. The two inertias and one capacitance between the two dashed rectangles represent the inertia of the second gear plus the inertia of the left half of the layshaft, the inertia of the third gear plus the inertia of the right half of the layshaft, and the torsional compliance of the layshaft. The fourth gear inertia, the output shaft compliance, and the bearing resistance are to the far right. The two ellipses inside the dashed rectangles each have the bond graph structure shown in Fig. 3, which represents dynamics of meshing gears. Returning to Fig. 2, the bearing resistances related to the layshaft rotation are shown as two 'R' elements off the 0-junctions directly below and between the two dashed rectangles. Because these bearings are mounted to the box, the velocities for these bearings are the differences between the shaft angular velocity and the angular velocity of the gearbox's rigid body motion. These velocity differences are constructed by the 0-junctions.

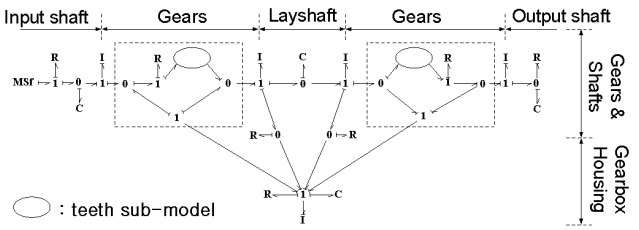

Figure 2 : Bond graph model of layshaft gearbox in Fig. 1[Kim (1999)]

3 Meshing gear teeth sub-model

Fig. 3, taken from reference [Kim and Bryant (1999)], is a bond graph model of tooth contact. This bond graph has symmetric upper and bottom parts, and symmetric right and left parts. The symmetry of upper and bottom parts represent the distribution of transmitted force between two pairs of teeth. In the case of low contact ratio ($1 <$ contact ratio < 2), the load on a given tooth is not constant, but is shared by another pair of teeth in contact. The tooth forces transmitted across a particular tooth pair depends on the angular position θ_1 of the pinion. These forces vanish when teeth separate. The signal from the ON/OFF switching signal element in the middle of the bond graph model conveys this information.

The right and left parts of the bond graph of Fig. 3, respectively describe the dynamic behavior of contacting teeth between driving and driven gears. Parame-

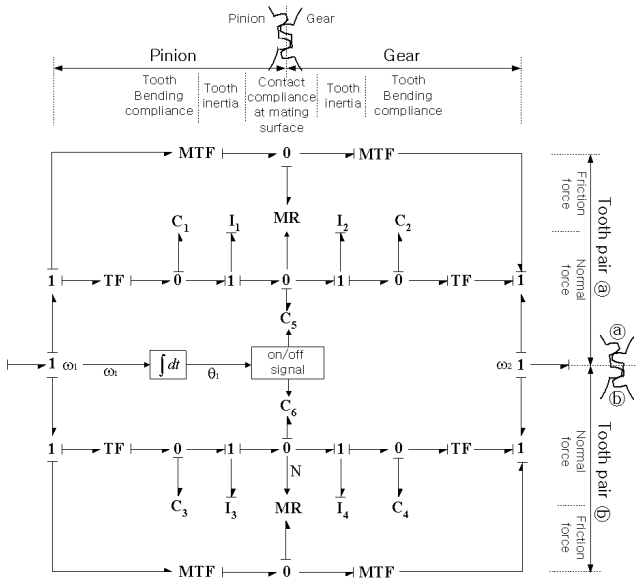

Figure 3 : Bond graph of a pair of meshing gears [Kim and Bryant (1999)]

ters C_1 through C_4 and I_1 through I_4 represent bending compliances (from beam theory) and equivalent masses of the two pairs of contacting gear teeth. Compliances C_5 and C_6 associated with surface contact between contacting gear teeth incorporate a nonlinear Hertzian contact stiffness that changes with angle θ_1 as the contact progresses over the tooth faces, consistent with the involute tooth profile. The MR resistance elements located on the vertical centerline represent the sliding friction losses between contacting gear teeth. The friction model is Coulomb, with normal force arising from the (Hertzian) contact compliance elements C_5 and C_6, and friction coefficient dependent on sliding speed. The two transformers (TF) on the left hand side convert the input torque from the pinion into normal forces between teeth, transmitted along the line of action. The two transformers (TF) on the right hand side act oppositely for the gear. Each modulated transformer (MTF) located on top and bottom left, converts pinion rotational velocity ω_1 into linear velocity tangential to tooth surfaces. Counterpart modulated transformers (MTF) to the right convert tangential velocities to rotational velocities ω_2. The 0-junctions in between the modulated transformers constructs the instantaneous sliding (slip) velocities associated with friction between contacting gear teeth.

4 Force onto shafts

To model energy storage due to bending of shafts generated from tooth contact forces, power bonds were added to Fig. 3. These groups of bonds and elements are shown in Fig. 4-(a), to the immediate right and left of the vertical centerline. For two meshing gears, power is transmitted to both shafts from both pairs of teeth via the gear attached to the shaft. Since the shafts are assumed linearly elastic, the applied forces and vibration motions separate into x and y components, shown in each group as 'shaft: x' and 'shaft: y'.

Normal and friction forces between teeth transfer to the gear bodies, and then to the shafts. The normal loads F_n are directed along the pressure line of action between contacting teeth, and the friction forces F_t are perpendicular to the normal forces F_n. The multi-port transformers contained in the new group of elements in Fig. 4-(a) perform coordinate system rotations ϕ from the n-t tooth system to the x-y shaft system shown in Fig. 4-(b). The forces and velocities transform according to

$$\begin{bmatrix} F_x \\ F_y \end{bmatrix} = \begin{bmatrix} \cos\phi & -\sin\phi \\ \sin\phi & \cos\phi \end{bmatrix} \begin{bmatrix} F_n \\ F_t \end{bmatrix}, \quad \begin{bmatrix} v_n \\ v_t \end{bmatrix} = \begin{bmatrix} \cos\phi & \sin\phi \\ -\sin\phi & \cos\phi \end{bmatrix} \begin{bmatrix} v_x \\ v_y \end{bmatrix} \tag{1}$$

where the angle ϕ is the pressure angle for the gears.

5 Finite element bending of shafts in bond graphs

5.1 Layshaft

To analyze dynamics of distributed shafts, concepts of finite elements will be adopted. Since the shafts were assumed linearly elastic, the bond graph module derived here for x directed bending motions apply to y directed bending motions also. In Fig. 5, the layshaft is considered composed of four beam bending elements, giving five nodes each with a linear displacement transverse to the shaft, and an out of plane rotation.

The bending displacement for the uniform element in Fig. 5-(a) is expressed using the standard beam shape

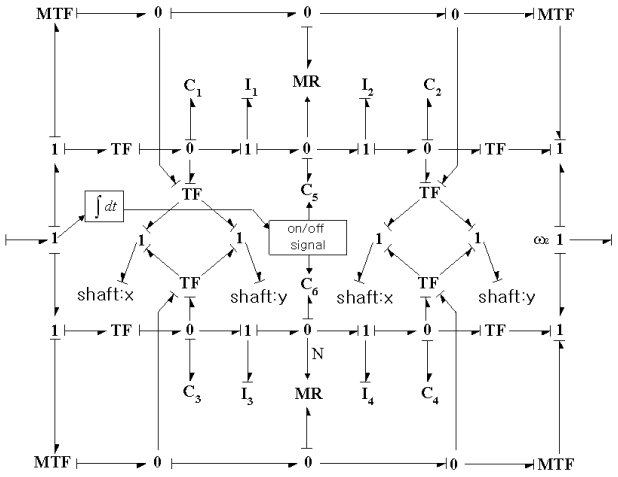

(a)

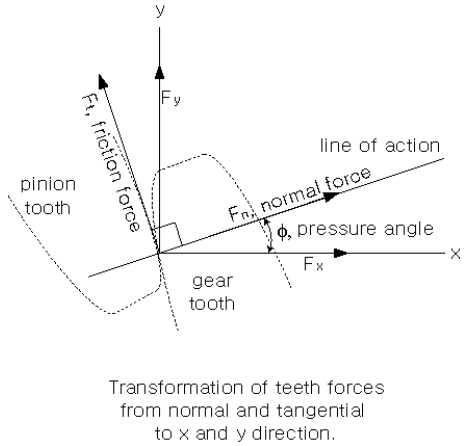

Transformation of teeth forces from normal and tangential to x and y direction.

(b)

Figure 4 : Teeth sub model with the power flow path to the shafts.

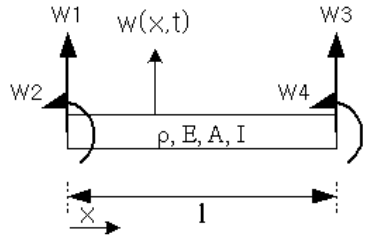

(a) uniform beam element

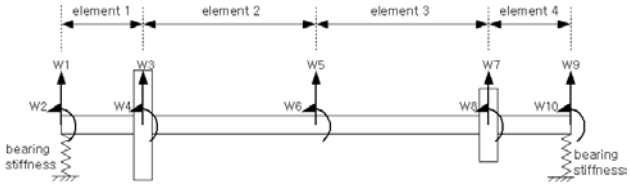

(b) 4 elements for the layshaft with two gears

Figure 5 : Finite element model of layshaft and notation of nodal displacement

functions, $L_i(x)$ as

$$w(x,t) = L_1(x)w_1(t) + L_2(x)w_2(t) + L_3(x)w_3(t) + L_4(x)w_4(t)$$

$$= (1 - 3\frac{x^2}{l^2} + 2\frac{x^3}{l^3})w_1(t) + (\frac{x}{l} - 2\frac{x^2}{l^2} + 3\frac{x^3}{l^3})lw_2(t)$$

$$+ (3\frac{x^2}{l^2} - 2\frac{x^3}{l^3})w_3(t) + (-\frac{x^2}{l^2} + \frac{x^3}{l^3})lw_4(t) \quad (2)$$

With these displacements, the element kinetic co-energy and potential energy are

$$T(t) = \frac{1}{2}\int_0^l \rho A \left\{\frac{\partial w(x,t)}{\partial t}\right\}^2 dx \equiv \frac{1}{2}\{\underline{\dot{w}}(t)\}^T[m]\{\underline{\dot{w}}(t)\}$$
$$V(t) = \frac{1}{2}\int_0^l EI \left\{\frac{\partial^2 w(x,t)}{\partial x^2}\right\}^2 dx \equiv \frac{1}{2}\{\underline{w}(t)\}^T[k]\{\underline{w}(t)\} \quad (3)$$

where the element mass and stiffness matrices are

$$[m] = \frac{\rho Al}{420}\begin{bmatrix} 156 & 22l & 54 & -13l \\ 22l & 4l^2 & 13l & -3l^2 \\ 54 & 13l & 156 & -22l \\ -13l & -3l^2 & -22l & 4l^2 \end{bmatrix} \quad (4)$$

$$[k] = \frac{EI}{l^3}\begin{bmatrix} 12 & 6l & -12 & 6l \\ 6l & 4l^2 & -6l & 2l^2 \\ -12 & -6l & 12 & -6l \\ 6l & 2l^2 & -6l & 4l^2 \end{bmatrix} \quad (5)$$

For assembly, we introduce an extended element nodal displacement vector $\{W\}_i$, equal to vector $\{w\}_i$ with as many zero components appended to make the dimension equal to N, the total number of nodal displacements of the complete system [Meirovitch (1986)]. Similarly, we extend the element mass matrix $[M]_i$ and element stiffness matrix $[K]_i$. The total kinetic co-energy and potential energy of the complete system is

$$T(t)=\tfrac{1}{2}\sum_{i=1}^{n}\{\underline{\dot{W}}(t)\}_i^T[\underline{M}]_i\{\underline{\dot{W}}(t)\}_i=\tfrac{1}{2}\{\underline{\dot{W}}(t)\}^T[M]\{\underline{\dot{W}}(t)\}$$
$$V(t)=\tfrac{1}{2}\sum_{i=1}^{n}\{\underline{W}(t)\}_i^T[\underline{K}]_i\{\underline{W}(t)\}_i=\tfrac{1}{2}\{\underline{W}(t)\}^T[K]\{\underline{W}(t)\} \quad (6)$$

where $[M]=\sum_{i=1}^{n}[\underline{M}]_i$ and $[K]=\sum_{i=1}^{n}[\underline{K}]_i$ are the 10×10 symmetric mass and stiffness matrices for the complete 4-element system. The kinetic co-energy given in equation (6) is a function of the velocity (or flow) variables

$$\underline{f}=\{\underline{\dot{W}}(t)\} \quad (7)$$

Bond graph inertances in integral causality have constitutive laws $f_i=f_i(\underline{p})$ wherein the flows $\underline{f}=[f_i]$ depend on the momentum variables $\underline{p}=[p_j]$ where $i, j = 1, 2,\ldots, n$. To obtain this constitutive law, we require the kinetic energy $T_*=T_*(\underline{p})$. From the Legendre transform [Kreyszig (1988)], the kinetic energy $T_*=T_*(\underline{p})$ and the kinetic co-energy $T=T(\underline{f})$ are related via

$$T_*(\underline{p})+T(\underline{f})=\underline{p}\cdot\underline{f} \quad (8)$$

Partial derivatives of equation (8) with respect to flow vector components f_i gives

$$p_i=\frac{\partial(\underline{p}\cdot\underline{f})}{\partial f_i}=\frac{\partial T(\underline{f})}{\partial f_i}\equiv P(\underline{f}) \quad (9)$$

In general, for application to bond graphs, equation (9) must be inverted, i.e.

$$\underline{f}=P^{-1}(p_i) \quad (10)$$

Substitutions of equations (4) and (6) into equation (9) gives

$$\underline{p}=[M]\left\{\dot{W}(t)\right\}=[M]\underline{f} \quad (11)$$

Equation (11) presents the momenta $\underline{p}$ as a linear function of flow $\underline{f}$. Inversion of equation (11) gives

$$\underline{f}=\underline{f}(\underline{p})=[M]^{-1}\underline{p} \quad (12)$$

as the constitutive law for the inertance of the finite element shaft in the bond graph.

The gear-attached layshaft system which has inertance and compliance can be expressed in bond graph form using multi port I and C elements. This bond graph, shown in Fig. 6, accounts for only x-motions. Another identical model was introduced into the complete system for y-motions. In Fig. 6, the flows on each 1-junction are time derivatives of the respective modal displacements. Odd numbered 1-junctions represent translations, even numbered 1-junctions represent rotations. Because the transverse displacements of the first and the last elements are influenced by the bearing stiffness, two power bonds are connected to the 1^{st} and 9^{th} nodal displacement 1-junctions. Likewise, gear forces generated from the tooth contacts are applied to the 2^{nd} and 4^{th} nodes in Fig. 5, shown as the power bonds on the 3^{rd} and 7^{th} 1-junctions.

Although only 4 elements were used, important natural frequencies and vibration modes can be estimated. Higher order frequencies and modes can be analyzed by incorporating more elements. Using the material and geometrical properties of the two gears and layshaft shown in Tab. 1, the mass and stiffness matrices were calculated.

The structure of Fig. 6, a multiport C interacting with a multiport I through 1-junctions, instills the FEM model into a bond graph. Each 1-junction can be associated with the time derivative of a nodal displacement of Fig. 5. These 1-junctions also program into the bond graph dynamic equilibrium between moments and forces at each node, provided by gear forces, bearing reactions, and the multiport I and C, which involve the mass and stiffness matrices. The bond graph of Fig. 6 shows how these effects interact with the rest of the physical system, and how motion equations should be derived. From this structure was derived the matrix differential equations of equation (17), and the interaction terms of equation (13). These will be presented later.

5.2 Input and output shafts

Bending of input and output shafts can be modeled in a similar manner. For the input shaft, only one reaction force arises from gear 1. Likewise, one reaction force

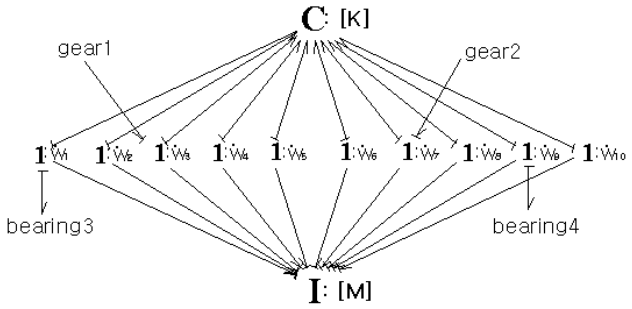

Figure 6 : Finite element, multi port model of gear-attached layshaft system

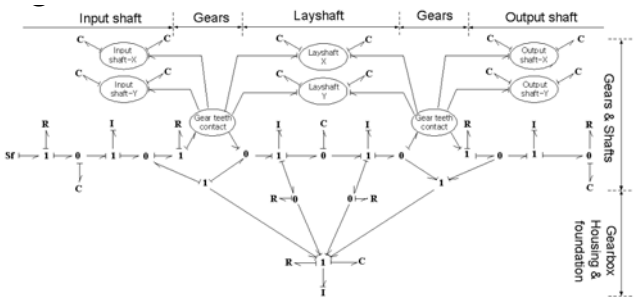

Figure 7 : Complete gearbox model, including all sub models

Table 1 : Material and geometrical properties of two gears and layshaft

Mass [kg]	1.920	4.184
I_{xx}- Mass Moment of Inertia [kg]	0.001969	0.004291
I_{zz}- Mass Moment of Inertia [kg]	0.003811	0.01810
Density of carbon steel or alloy steel [kg/m^3]	7.70E+03	
Young's modulus of carbon steel or alloy steel [Pa]	2.10E+11	
Lay shaft length [m]	0.1+0.2+0.2+0.1	
Lay shaft radius [m]	0.01	
Layshaft area moment of inertia [m^4]	7.85E-09	
Layshaft cross sectional area [m^2]	3.14E-04	

arises from gear 4 on the output shaft. Each shaft is supported by two bearings, and bonds that transfer power from shaft to bearing should be attached to each bond graph/FEM shaft sub-model. As in the layshaft model, only four finite elements were considered.

5.3 Combining sub-models into a complete model

Utilizing the modular characteristics of bond graphs, sub-models can be linked. The complete gearbox model shown in Fig. 7 is the model of Fig. 1 with two teeth contact sub-models, two layshaft bending sub-models (for x and y motions), two input shaft bending sub-models, and two output shaft bending sub-models. State equations were extracted from the entire gearbox model in Fig. 7. These equations are presented in Appendix A. The state variables are defined in the nomenclature.

6 Numerical methods

6.1 1st order state equations from bond graph

State equations from the lumped parameter section of the bond graph can be expressed in the matrix equation form,

$$\dot{X} = BX + P\dot{D} + F \tag{13}$$

Here, the state vector X consists of all the state variables of Appendix A, matrix P incorporates the effects of the (FEM) shaft bending onto the other components in the gearbox system, and F is the vector of input excitations (the velocity source). In equation (13), nodal velocities $\dot{D}$ appear instead of nodal displacements D, because the relevant equations arose from kinematics of velocities, rather than displacements. These kinematics are equivalent, since velocities are time derivatives of displacements.

At time t_{j+1}, the state equations can be written as

$$\begin{aligned} \dot{X}_{j+1} &= BX_{j+1} + P\dot{D}_{j+1} + F_{j+1} \\ &= BX_{j+1} + P\left(\dot{D}_j + \Delta\dot{D}_j\right) + F_{j+1} \end{aligned} \tag{14}$$

where,

$$\dot{X}_{j+1} = \frac{(X_{j+1} - X_j)}{\Delta t} \tag{15}$$

was approximated by backward difference, and $\Delta\dot{D}_j$, the vector of nodal velocity increments over time steps Δt, derived from Newmark's method, is explained in Appendix B. Term $\dot{D}_j$ is the vector of nodal velocities at time t_j.

Now substitute equations (B.10) from the Appendix B and (15) into the state equations of motion, (14) to obtain

$$\frac{(X_{j+1}-X_j)}{\Delta t} = BX_{j+1} + P\dot{D}_j + \frac{\gamma}{\beta\Delta t}P\Delta D_j - P\hat{R}_j + F_{j+1}.$$

Here, β and γ are numerical parameters of Newmark's method and ΔD_j is the vector of nodal displacement increments.

Collecting terms,

$$\begin{aligned} -\frac{\gamma}{\beta\Delta t}P\Delta D_j + \left(\frac{1}{\Delta t}I - B\right)X_{j+1} \\ = P\left(\dot{D}_j - \hat{R}_j\right) + \frac{1}{\Delta t}X_j + F_{j+1} \end{aligned} \tag{16}$$

In this case, the unknowns ΔD_j and X_{j+1} are grouped on the left hand side of equation (16).

6.2 2^{nd} order matrix equations from finite elements

Second order matrix ordinary differential equations were extracted from the 1-junctions between interacting multiport I and C's, as in Fig. 6.

From the inertance bonds arose equation

$$\dot{P} = -KD + A$$

and from capacitance bonds arose

$$\dot{D} = M^{-1}P.$$

By differentiating the second of these equations, and substituting the second into the first, we obtain a matrix differential system in displacement variable D,

$$M\ddot{D} + KD = A = a + QX \tag{17}$$

where, a is the input force vector to the finite element part and Q is the matrix which relates the finite element to the lumped parameter bond graph part. We chose to use second order matrix differential equations, rather than state equations normally extracted from bond graphs, to avoid calculating the inverse of the mass matrix, implied by equation (12). This would destroy the sparseness of the mass matrix, key to quick and efficient solution of finite elements.

Equation (17) reduces to

$$\hat{K}\Delta D_j = \Delta\hat{A}_j \tag{18}$$

via Newmark's algorithm, where

$$\begin{aligned} \Delta\hat{A}_j &= \Delta A_j + M\hat{Q}_j \\ &= (\Delta a_j + Q_{j+1}X_{j+1} + Q_jX_j) + M\hat{Q}_j \end{aligned} \tag{19}$$

Substitution of equation (19) into equation (18), and arranging terms, gives

$$\hat{K}\Delta D_j - Q_{j+1}X_{j+1} = \Delta a_j + Q_jX_j + M\hat{Q}_j \tag{20}$$

The unknowns ΔD_j and X_{j+1} are on left hand side of equation (20).

6.3 Combined system

Assembling from equations (16) and (20) into matrix form gives

$$\begin{aligned} &\begin{bmatrix} \hat{K} & -Q_{j+1} \\ -\frac{\gamma}{\beta\Delta t}P & \frac{1}{\Delta t}I - B \end{bmatrix} \begin{bmatrix} \Delta D_j \\ X_{j+1} \end{bmatrix} \\ &= \begin{bmatrix} \Delta a_j - Q_jX_j + M\hat{Q}_j \\ P\left(\dot{D}_j - \hat{R}_j\right) + \frac{1}{\Delta t}X_j + F_{j+1} \end{bmatrix} \end{aligned} \tag{21}$$

At each step of the calculation, we can solve the unknowns ΔD_j and X_{j+1}; then D_{j+1}, $\dot{D}_{j+1}$, and $\ddot{D}_{j+1}$ can be solved by equations (B.16), (B.17), and (B.18) from the Appendix B during an auxiliary step. Before the next step of calculation,

$\hat{Q}_j$and $\hat{R}_j$ also must be updated using equations (B.11) and (B.12) from the Appendix B.

6.4 Simple example of Combination of 1^{st} and 2^{nd} order systems

Fig. 8 is a schematic of a system and its bond graph which has finite element shaft bending, and lumped parameter elements (mass m_a and stiffness k_a, k_{br1}, and

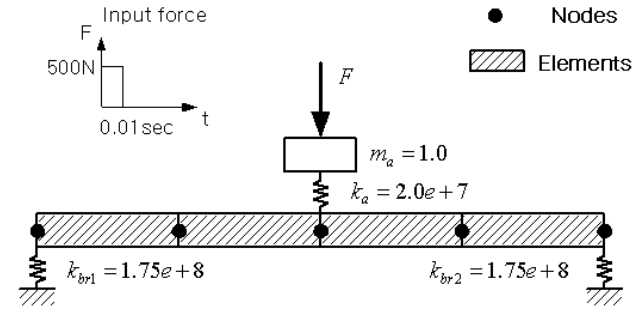

(a) Example physical model

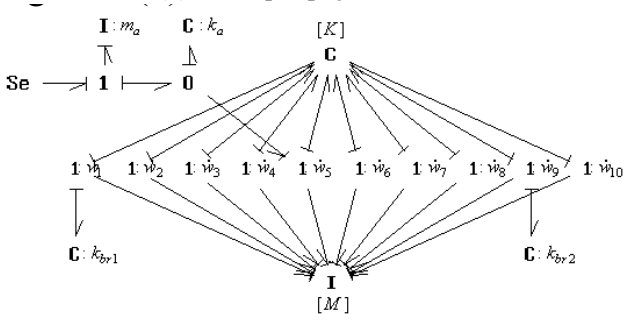

(b) Bond graph expression of (a)

Figure 8 : Example model and the bond graph

k_{br2}). F is the input force. The same material, geometrical properties, and the finite element model as in Kim's thesis were applied. The results obtained using equation (21) coded and solved in MATLAB® are represented in Fig. 9-(a) and Fig. 10-(a) (Time step = 0.000005, $\gamma = 1/2$ and $\beta = 1/4$). For the purpose of comparison, the same example was solved by ANSYS® and plotted in Fig. 9-(b) and Fig. 10-(b).

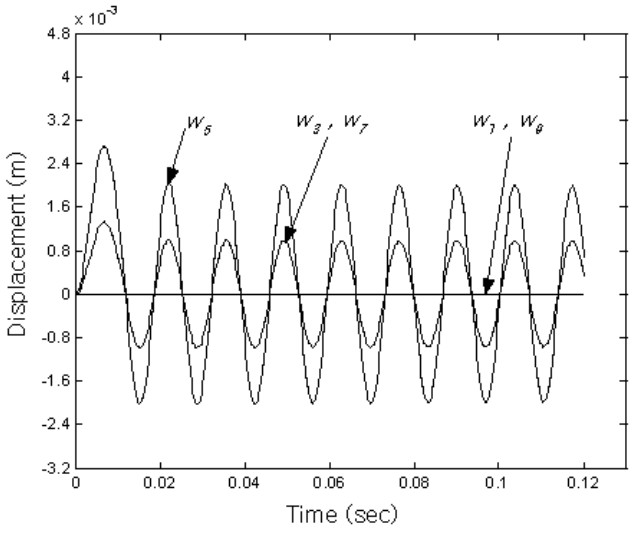

(a) Equation (21) and Newmark's algorithm

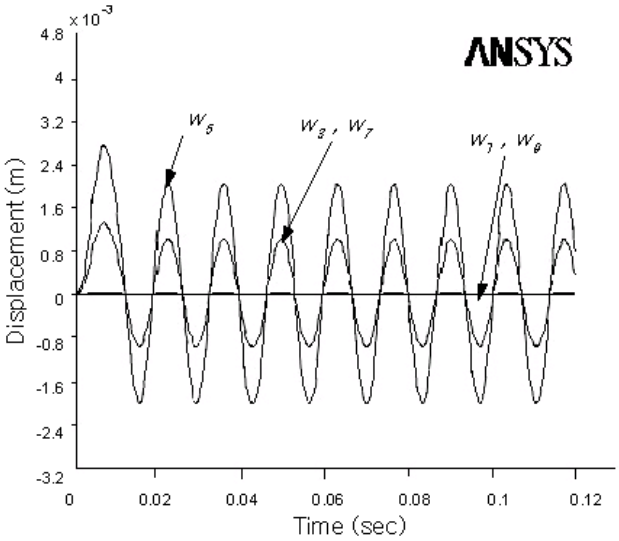

(b) ANSYS®

Figure 9 : Displacement of nodes

7 Simulation of a layshaft gearbox

7.1 Formulation for gearbox model

By extending the formulation to a finite element shaft bending model with many elements, the layshaft gearbox model in Fig. 7 can be simulated.

As in equation (13), state equations from the bond graph part can be represented as

$$\dot{X} = BX + F + P_1\dot{D}^{in\_x} + P_2\dot{D}^{in\_y} + P_3\dot{D}^{lay\_x} + P_4\dot{D}^{lay\_y} + P_5\dot{D}^{out\_x} + P_6\dot{D}^{out\_y} \quad (22)$$

where, P_1, P_2, P_3, P_4, P_5, and P_6 are matrices which relate the lumped parameter bond graph parts of the system to the finite element model part, Input shaft-X (in_x), Input shaft-Y (in_y), Layshaft-X (lay_x), Layshaft-Y (lay_y), Output shaft-X (out_x), and Output shaft-Y (out_y), respectively.

Versions of equation (17) describe each finite element matrix model for the input, lay, and output shaft bendings in the x and y directions.

By applying Newmark's procedures, equation (22) can be rearranged as

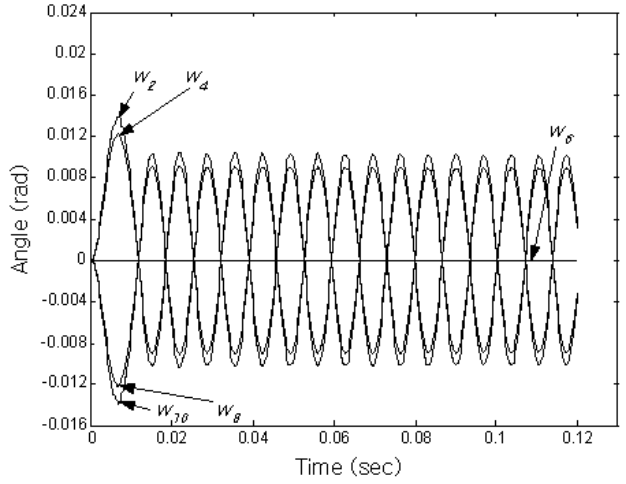

(a) Equation (21) and Newmark's algorithm

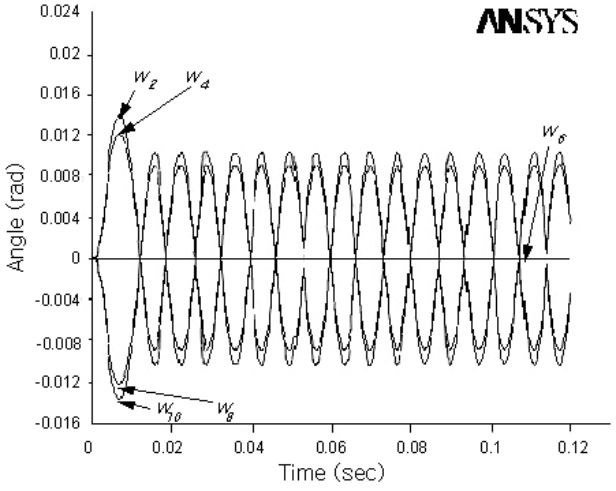

(b) ANSYS®

Figure 10 : Angles of nodes

$$
\begin{aligned}
&\hat{K}\Delta D_j^{in\_x} - Q_{j+1}^{in\_x}X_{j+1} = \Delta a_j^{in\_x} - Q_j^{in\_x}X_j + M\hat{Q}_j^{in\_x}\\
&\hat{K}\Delta D_j^{in\_y} - Q_{j+1}^{in\_y}X_{j+1} = \Delta a_j^{in\_y} - Q_j^{in\_y}X_j + M\hat{Q}_j^{in\_y}\\
&\hat{K}\Delta D_j^{lay\_x} - Q_{j+1}^{lay\_x}X_{j+1} = \Delta a_j^{lay\_x} - Q_j^{lay\_x}X_j + M\hat{Q}_j^{lay\_x}\\
&\hat{K}\Delta D_j^{lay\_y} - Q_{j+1}^{lay\_y}X_{j+1} = \Delta a_j^{lay\_y} - Q_j^{lay\_y}X_j + M\hat{Q}_j^{lay\_y}\\
&\hat{K}\Delta D_j^{out\_x} - Q_{j+1}^{out\_x}X_{j+1} = \Delta a_j^{out\_x} - Q_j^{out\_x}X_j + M\hat{Q}_j^{out\_x}\\
&\hat{K}\Delta D_j^{out\_y} - Q_{j+1}^{out\_y}X_{j+1} = \Delta a_j^{out\_y} - Q_j^{out\_y}X_j + M\hat{Q}_j^{out\_y}
\end{aligned}
\tag{24}
$$

Converting equations (23) and (24) into matrix form gives,

$$
\begin{bmatrix}
\hat{K} & [0] & [0] & [0] & [0] & [0] & -Q_{j+1}^{in\_x}\\
[0] & \hat{K} & [0] & [0] & [0] & [0] & -Q_{j+1}^{in\_y}\\
[0] & [0] & \hat{K} & [0] & [0] & [0] & -Q_{j+1}^{lay\_x}\\
[0] & [0] & [0] & \hat{K} & [0] & [0] & -Q_{j+1}^{lay\_y}\\
[0] & [0] & [0] & [0] & \hat{K} & [0] & -Q_{j+1}^{out\_x}\\
[0] & [0] & [0] & [0] & [0] & \hat{K} & -Q_{j+1}^{out\_y}\\
-\frac{\gamma}{\beta\Delta t}P_1 & -\frac{\gamma}{\beta\Delta t}P_2 & -\frac{\gamma}{\beta\Delta t}P_3 & -\frac{\gamma}{\beta\Delta t}P_4 & -\frac{\gamma}{\beta\Delta t}P_5 & -\frac{\gamma}{\beta\Delta t}P_6 & \frac{1}{\Delta t}I - B
\end{bmatrix}
\begin{bmatrix}
\Delta D_j^{in\_x}\\ \Delta D_j^{in\_y}\\ \Delta D_j^{lay\_x}\\ \Delta D_j^{lay\_y}\\ \Delta D_j^{out\_x}\\ \Delta D_j^{out\_y}\\ X_{j+1}
\end{bmatrix}
$$

$$
= \begin{bmatrix}
[\Delta a_j^{in\_x} - Q_j^{in\_x}X_j + M\hat{Q}_j^{in\_x}]\\
[\Delta a_j^{in\_y} - Q_j^{in\_y}X_j + M\hat{Q}_j^{in\_y}]\\
[\Delta a_j^{lay\_x} - Q_j^{lay\_x}X_j + M\hat{Q}_j^{lay\_x}]\\
[\Delta a_j^{lay\_y} - Q_j^{lay\_y}X_j + M\hat{Q}_j^{lay\_y}]\\
[\Delta a_j^{out\_x} - Q_j^{out\_x}X_j + M\hat{Q}_j^{out\_x}]\\
[\Delta a_j^{out\_y} - Q_j^{out\_y}X_j + M\hat{Q}_j^{out\_y}]\\
\begin{bmatrix}
P_1\left(\dot{D}_j^{in\_x} - \hat{R}_j^{in\_x}\right) + P_2\left(\dot{D}_j^{in\_y} - \hat{R}_j^{in\_y}\right) + P_3\left(\dot{D}_j^{lay\_x} - \hat{R}_j^{lay\_x}\right)\\
+P_4\left(\dot{D}_j^{lay\_y} - \hat{R}_j^{lay\_y}\right) + P_5\left(\dot{D}_j^{out\_x} - \hat{R}_j^{out\_x}\right) + P_6\left(\dot{D}_j^{out\_y} - \hat{R}_j^{out\_y}\right)\\
+\frac{1}{\Delta t}X_j + F_{j+1}
\end{bmatrix}
\end{bmatrix}
\tag{25}
$$

$$
\begin{aligned}
&-\tfrac{\gamma}{\beta\Delta t}(P_1\Delta D_j^{in\_x} + P_2\Delta D_j^{in\_y} + P_3\Delta D_j^{lay\_x} + P_4\Delta D_j^{lay\_y}\\
&+P_5\Delta D_j^{out\_x} + P_6\Delta D_j^{out\_y}) + (\tfrac{1}{\Delta t}I - B)X_{j+1} = \tfrac{1}{\Delta t}X_j + F_{j+1}\\
&+P_1\left(\dot{D}_j^{in\_x} - \hat{R}_j^{in\_x}\right) + P_2\left(\dot{D}_j^{in\_y} - \hat{R}_j^{in\_y}\right) + P_3\left(\dot{D}_j^{lay\_x} - \hat{R}_j^{lay\_x}\right)\\
&+P_4\left(\dot{D}_j^{lay\_y} - \hat{R}_j^{lay\_y}\right) + P_5\left(\dot{D}_j^{out\_x} - \hat{R}_j^{out\_x}\right) + P_6\left(\dot{D}_j^{out\_y} - \hat{R}_j^{out\_y}\right)
\end{aligned}
\tag{23}
$$

and equations (17) for the various shaft bendings become

By solving equation (25) and applying Newmark's algorithm, the layshaft gearbox model can be simulated.

7.2 Simulation results

Based on the bond graph model presented in Fig. 7, a simulation was performed in MATLAB® with a time step of 10^{-5} and the values of system parameters shown in Tab. 2 applied to both gear pairs.

The input to the flow source on the far left of Fig. 7 was a cycloidal step function from 0 to 50 rad/sec, starting at

Table 2 : Geometrical, material properties of spur gears, standard full depth tooth system

Parameter	Pinion	Gear
Module [mm]	6	
Number of teeth	21	31
Pressure Angle [degree]	20°	
Circular Pitch [mm] (=pi*module)	18.85	
[p_b] Base Pitch [mm]	17.713	
[r_p] Pitch Circle radius [mm]	63	93
[r_b] Base Circle radius [mm] (=Pitch Circle radius*cos(Pressure Angle))	59.2	87.4
Center Distance [mm]	156	
Addendum [mm] (=module)	6	
Deddendum [mm] (=1.25*module)	7.5	
[m_c= (u_a+u_r)/ p_b] Contact Ratio	1.615	
Face width [mm]	20	
I_{zz}– Mass Moment of Inertia [kg]	0.00381	0.0181
Density of carbon steel or alloy steel [kg/m^3]	7.70E+03	
Young's modulus of carbon steel or alloy steel [Pa]	2.10E+11	
Friction coefficient between teeth	0.005	

t_s=0 sec and ending at t_e=0.5 sec. A mathematical description of this signal is

$$\Delta t = \frac{2\pi(t - t_s)}{t_e - t_s} \tag{26}$$

$$\Omega_{out} = \begin{cases} \Omega_{Min} & ;\Delta t < 0 \\ \Omega_{Min} + (\Omega_{Max} - \Omega_{Min})\frac{\Delta t - \sin(\Delta t)}{2\pi} & ;0 \le \Delta t \le 2\pi \\ \Omega_{Max} & ;\Delta t > 2\pi \end{cases} \tag{27}$$

where

Ω_{Min}	Starting value of the output signal. (0 rad/sec)
Ω_{Max}	End value of the output signal. (50 rad/sec)
t_s	Start time of the cycloid. (0 sec)
t_e	End time of the cycloid. (0.5 sec)

This cycloidal function is smoother and physically more reasonable than a step input, which will generate enormous forces at the step change. The input cycloidal angular velocity and load sharing ratio are represented in Fig. 11. The angular velocity ratio between input and output

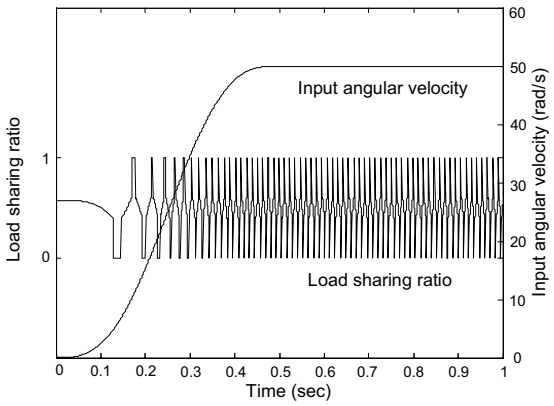

Figure 11 : Cyclodial input angular velocity and load sharing ratio

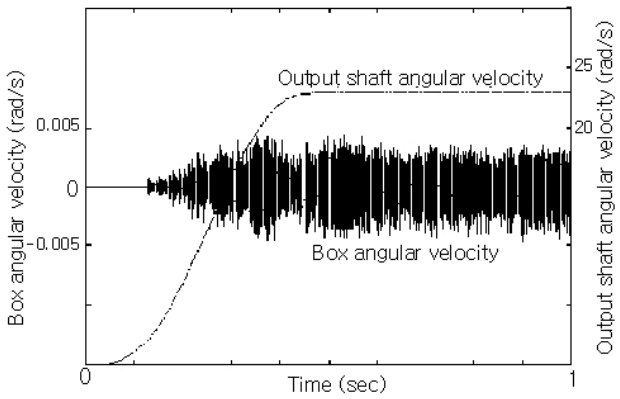

(a) Output velocity and box vibration

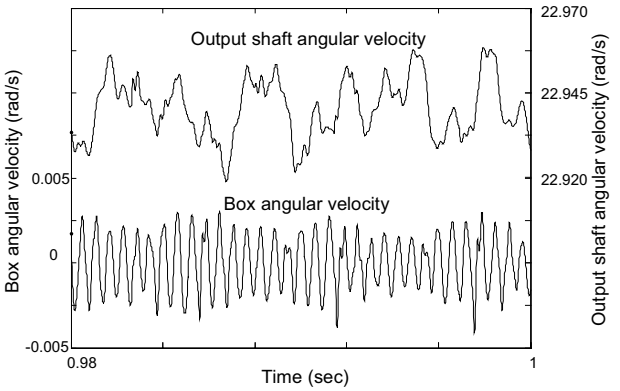

(b) Magnified plot of (a)

Figure 12 : Output velocity of layshaft gearbox and box vibration

shaft must be $(21/31)^2$ + (transmission errors) in accordance with the teeth number ratio or pitch circle radii ratio for two pairs of mating gears. The simulation results shown in Fig. 12 reflect this ratio of input and output shaft velocities, and transmission errors.

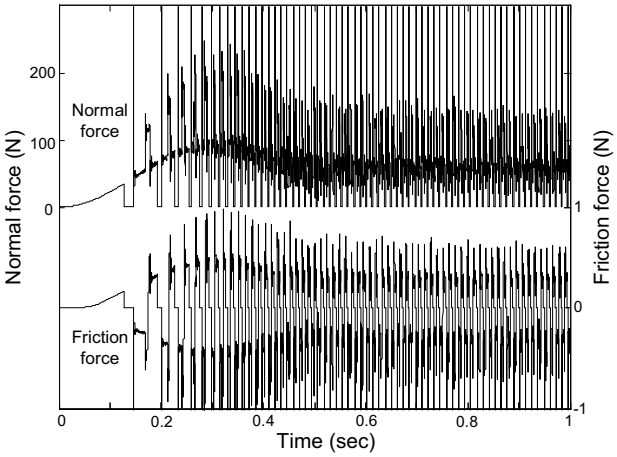

(a) Normal and friction forces

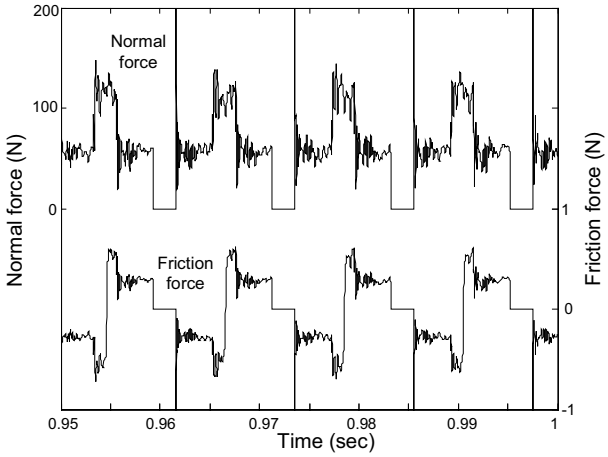

(b) Magnified plot of (a)

Figure 13 : Normal and friction forces between surface of meshing gears

In this simulation, the angular velocity input is a flow source with a cycloidal step function having 50 rad/s amplitude. The average power transmitted across the gearbox is 825 W with average steady state input torque 16.5 N·m. If all components are rigid bodies, the expected output velocity is $50*(21/31)^2$ = 22.945 rad/s. To compare this value with the simulation results, a portion of

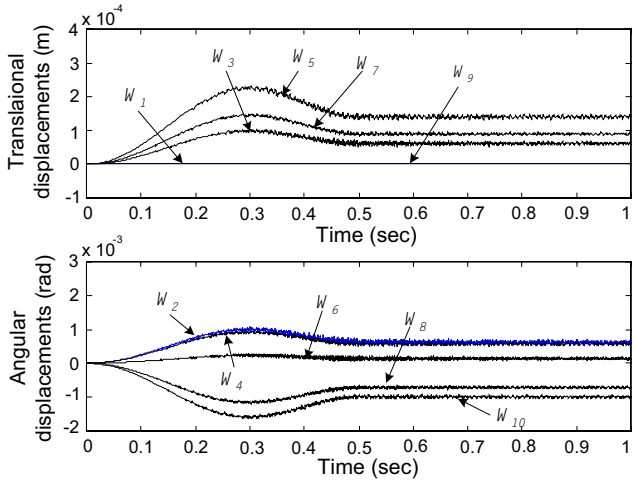

(a) Input shaft

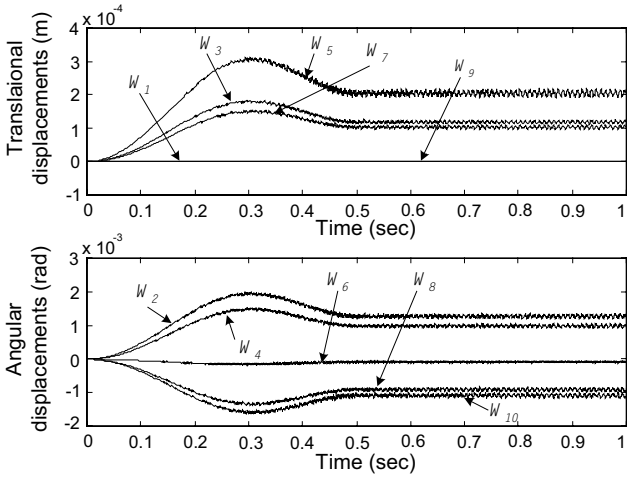

(b) Layshaft

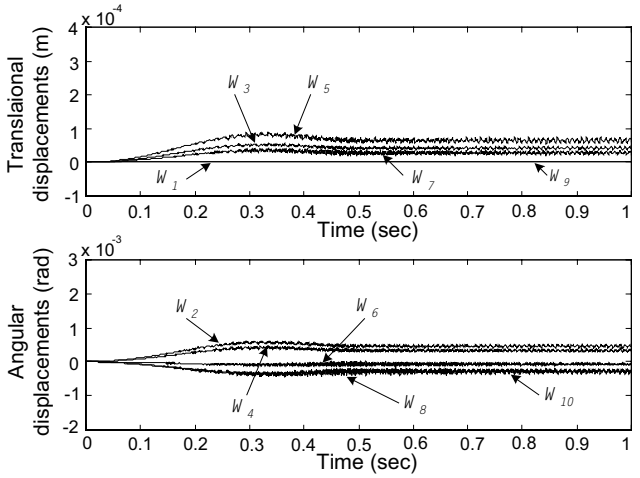

(c) Output shaft

Figure 14 : x-direction shafts bending at each node

Fig. 12-(a) was magnified in Fig. 12-(b). The actual output velocity in Fig. 12-(b) oscillates between 22.92 rad/s and 22.97 rad/s due to transmission errors caused by tooth bending compliances, compliances of shafts, and contact mechanisms. These transmission errors will not decay, because the number of pairs of teeth in contact fluctuates between 1 and 2. This creates impact loads which activate oscillations. Moreover, the effective stiffness of teeth bending and teeth in contact will increase whenever teeth are in contact. The forces between contacting teeth of meshing gears are represented in Fig. 13. Here gears meshing in sequence with the load sharing ratio act like impact sources.

Fig. 14 shows the response of each node (1-junction) of the finite element shafts. The x-direction movements of each shaft in Fig. 7 were plotted. The y-direction movements had similar tendencies. We can see that the center of each shaft has the largest translational displacement (w_5), but the smallest value of angular displacement (w_6). Both ends of each shaft have the smallest translational displacement (w_1 and w_9), but the largest angular displacement (w_2 and w_{10}) because the bearings at both ends restrain the shaft displacements. Each shaft bends in a bow shape with high frequency bending vibrations.

8 Summary and conclusions

We presented an updated bond graph model of a gearbox, which now includes bending of shafts. To analyze shaft dynamics more precisely, elementary finite element theory was adopted. The complete model was simulated, using numerical methods derived via state equations from bond graph model, and Newmark-β method for lumped and finite element techniques.

The updated model can simulate the dynamic behavior of gear teeth, shafts, gearbox housing, and interactions. This gearbox model will be used in such fields as fault diagnosis and control, which need detailed descriptions of dynamics.

Acknowledgement: The authors would like to thank the National Science Foundation, Grant DMI-9713605, Manufacturing Machines and Equipment Program, Atoztec System Inc. of Hong Kong, China, and the Texas Higher Education Board, Grant ATP 003658-0295-1999 for support.

References

Hrovat, D.; Tobler, W. E. (1991): Bond graph modeling of automotive power trains, *Journal of the Franklin Institute*, vol. 328, pp. 623-662.

Karnopp, D. C.; Margolis, D. L.; Rosenberg, R. C. (2000): *System Dynamics: Modeling and Simulation of Mechatronic System, 3rd edition*, Wiley, New York.

Kim, J. (1999): Bond Graph models of a squirrel-cage induction motor and a Layshaft gearbox for degradation analysis, *Master thesis*, The University of Texas – Austin.

Kim, J.; Bryant, M. D. (1999): A Bond Graph Model of Gear Tooth Contacts and Effects of Vibration on Tooth Surface Failure, *The Advancing Frontiers of Engineering Tribology, Proceedings of the 1999 STLE/ASME H.S. Cheng Tribology Surveillance*, pp. 163-175.

Kreyszig, E. (1988): *Advanced Engineering Mathematics, 6th ed.*, John Wiley & Sons, New York.

Meirovitch, L. (1986): *Elements of vibration analysis*, McGraw-Hill, New York, pp. 318.

Özgüven, H. N.; Houser, D. R. (1988): Mathematical Models Used In Gear Dynamics - A Review, *Journal of Sound and Vibration*, vol. 82, pp. 383-411.

Paynter, H. M. (1960): *Analysis and Design of Engineering Systems*, M.I.T Press, Cambridge, Mass.

Weaver, W. Jr.; Johnston, P. R. (1987): *Structural Dynamics by Finite Elements*, Prentice-Hall, pp. 218-220.

Appendix A: Bond graph models with index and state equations

A.1 Bond graph models with index

A.1.1 Gear teeth contact sub-model

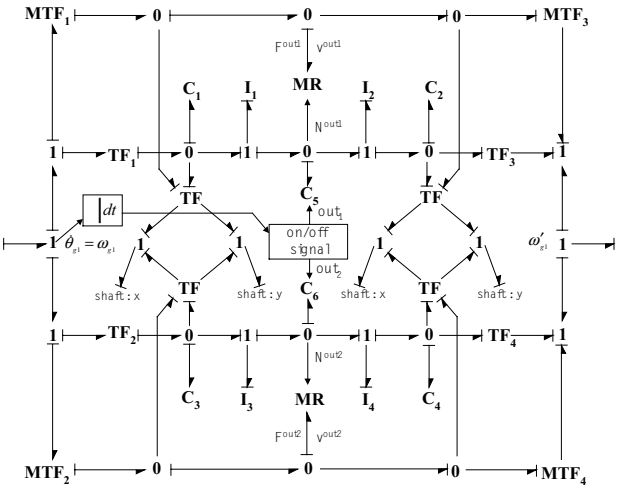

A.1.2 Parameters of gear teeth contact sub-model

Parameters	Description	Value
$\mathbf{I_1, I_2, I_3, I_4}$	Equivalent mass of gear [kg]	0.001587
$\mathbf{C_1, C_2, C_3, C_4}$	Bending compliance of gear [m/N]	9.203e-9
$\mathbf{C_5, C_6}$	Compliace of gear teeth contact [m/N]	2.76e-10
$\mathbf{TF_1, TF_2}$	Transformer (rotational to translational)	0.0592
$\mathbf{TF_3, TF_4}$	Transformer (translational to rotational)	11.4416

A.1.3 Layshaft gearbox model

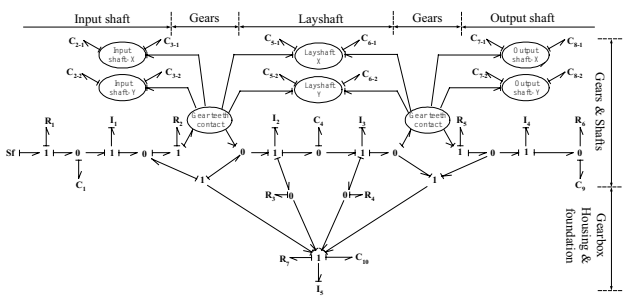

A.1.4 Parameters of gearbox housing and shafts

Parameters	Description	Value
$\mathbf{I_1, I_2, I_3, I_4}$	Rotational inertia of shaft [kg·m^2]	0.03
$\mathbf{I_5}$	Rotational inertia of gearbox [kg·m^2]	0.3
$\mathbf{C_1, C_4, C_9}$	Torsional compliance of shaft [rad/N·m]	2e-7
$\mathbf{C_{10}}$	Torsional compliance of gearbox [rad/N·m]	5e-8
$\mathbf{R_1, R_2, R_3, R_4, R_5, R_6}$	Rotational resistance of bearing [N·m·sec]	0.1
$\mathbf{R_7}$	Gearbox damping [N·m·sec]	0.1
$\mathbf{C_{2\text{-}1}, C_{2\text{-}2}, C_{3\text{-}1}, C_{3\text{-}2}}$ $\mathbf{C_{5\text{-}1}, C_{5\text{-}2}, C_{6\text{-}1}, C_{6\text{-}2}}$ $\mathbf{C_{7\text{-}1}, C_{7\text{-}2}, C_{8\text{-}1}, C_{8\text{-}2}}$	Compliance of bearing at shaft [m/N]	5.7e-9

A.2 State equations

The subscripts g_1 and g_2 represent gear teeth contact sub-models (oval shape) of the left and right hand side in layshaft gearbox model, respectively.

A.2.1 Gear teeth contact sub-model: left hand side

$$\dot{\theta}_{g_1} = \frac{1}{I_1}h_{I_1} + \frac{1}{I_5}h_{I_5}$$

$$\dot{q}_{g_1\_c_1} = (TF_1)_{g_1}\left(\frac{1}{I_1}h_{I_1} + \frac{1}{I_5}h_{I_5}\right) - \frac{1}{I_{g_1\_i_1}}P_{g_1\_i_1} - \cos\phi\dot{D}_{in\_x\_7} - \sin\phi\dot{D}_{in\_y\_7}$$

$$\dot{P}_{g_1\_i_1} = \frac{1}{C_{g_1\_c_1}}q_{g_1\_c_1} - \frac{(out_1)_{g_1}}{C_{g_1\_c_2}}q_{g_1\_c_2}$$

$$\dot{q}_{g_1\_c_2} = \frac{1}{I_{g_1\_i_1}}P_{g_1\_i_1} - \frac{1}{I_{g_1\_i_2}}P_{g_1\_i_2}$$

$$\dot{P}_{g_1\_i_2} = \frac{(out_1)_{g_1}}{C_{g_1\_c_2}}q_{g_1\_c_2} - \frac{1}{C_{g_1\_c_3}}q_{g_1\_c_3}$$

$$\dot{q}_{g_1\_c_3} = \frac{1}{(TF_3)_{g_1}}\left(-\frac{1}{I_2}h_{I_2} + \frac{1}{I_5}h_{I_5}\right) + \frac{1}{I_{g_1\_i_2}}P_{g_1\_i_2} - \cos\phi\dot{D}_{lay\_x\_3} - \sin\phi\dot{D}_{lay\_y\_3}$$

$$\dot{q}_{g_1\_c_4} = (TF_2)_{g_1}\left(\frac{1}{I_1}h_{I_1} + \frac{1}{I_5}h_{I_5}\right) - \frac{1}{I_{g_1\_i_3}}P_{g_1\_i_3} - \cos\phi\dot{D}_{in\_x\_7} - \sin\phi\dot{D}_{in\_y\_7}$$

$$\dot{P}_{g_1\_i_3} = \frac{1}{C_{g_1\_c_4}}q_{g_1\_c_4} - \frac{(out_2)_{g_1}}{C_{g_1\_c_5}}q_{g_1\_c_5}$$

$$\dot{q}_{g_1\_c_5} = \frac{1}{I_{g_1\_i_3}}P_{g_1\_i_3} - \frac{1}{I_{g_1\_i_4}}P_{g_1\_i_4}$$

$$\dot{P}_{g_1\_i_4} = \frac{(out_2)_{g_1}}{C_{g_1\_c_5}}q_{g_1\_c_5} - \frac{1}{C_{g_1\_c_6}}q_{g_1\_c_6}$$

$$\dot{q}_{g_1\_c_6} = \frac{1}{(TF_4)_{g_1}}\left(-\frac{1}{I_2}h_{I_2} + \frac{1}{I_5}h_{I_5}\right) + \frac{1}{I_{g_1\_i_4}}P_{g_1\_i_4} - \cos\phi\dot{D}_{lay\_x\_3} - \sin\phi\dot{D}_{lay\_y\_3}$$

A.2.2 Gear teeth contact sub-model: right hand side

$$\dot{\theta}_{g_2} = \frac{1}{I_3}h_{I_3} - \frac{1}{I_5}h_{I_5}$$

$$\dot{q}_{g_2\_c_1} = (TF_1)_{g_2}\left(\frac{1}{I_3}h_{I_3} - \frac{1}{I_5}h_{I_5}\right) - \frac{1}{I_{g_2\_i_1}}P_{g_2\_i_1} - \cos\phi\dot{D}_{lay\_x\_7} - \sin\phi\dot{D}_{lay\_y\_7}$$

$$\dot{P}_{g_2\_i_1} = \frac{1}{C_{g_2\_c_1}}q_{g_2\_c_1} - \frac{(out_1)_{g_2}}{C_{g_2\_c_2}}q_{g_2\_c_2}$$

$$\dot{q}_{g_2\_c_2} = \frac{1}{I_{g_2\_i_1}}P_{g_2\_i_1} - \frac{1}{I_{g_2\_i_2}}P_{g_2\_i_2}$$

$$\dot{P}_{g_2\_i_2} = \frac{(out_1)_{g_2}}{C_{g_2\_c_2}}q_{g_2\_c_2} - \frac{1}{C_{g_2\_c_3}}q_{g_2\_c_3}$$

$$\dot{q}_{g_2\_c_3} = -\frac{1}{(TF_3)_{g_2}}\left(\frac{1}{I_4}h_{I_4} + \frac{1}{I_5}h_{I_5}\right) + \frac{1}{I_{g_2\_i_2}}P_{g_2\_i_2} - \cos\phi\dot{D}_{out\_x\_3} - \sin\phi\dot{D}_{out\_y\_3}$$

$$\dot{q}_{g_2\_c_4} = (TF_2)_{g_2}\left(\frac{1}{I_3}h_{I_3} - \frac{1}{I_5}h_{I_5}\right) - \frac{1}{I_{g_2\_i_3}}P_{g_2\_i_3} - \cos\phi\dot{D}_{lay\_x\_7} - \sin\phi\dot{D}_{lay\_y\_7}$$

$$\dot{P}_{g_2\_i_3} = \frac{1}{C_{g_2\_c_4}}q_{g_2\_c_4} - \frac{(out_2)_{g_2}}{C_{g_2\_c_5}}q_{g_2\_c_5}$$

$$\dot{q}_{g_2\_c_5} = \frac{1}{I_{g_2\_i_3}}P_{g_2\_i_3} - \frac{1}{I_{g_2\_i_4}}P_{g_2\_i_4}$$

$$\dot{P}_{g_2\_i_4} = \frac{(out_2)_{g_2}}{C_{g_2\_c_5}}q_{g_2\_c_5} - \frac{1}{C_{g_2\_c_6}}q_{g_2\_c_6}$$

$$\dot{q}_{g_2\_c_6} = -\frac{1}{(TF_4)_{g_2}}\left(\frac{1}{I_4}h_{I_4} + \frac{1}{I_5}h_{I_5}\right) + \frac{1}{I_{g_2\_i_4}}P_{g_2\_i_4} - \cos\phi\dot{D}_{out\_x\_3} - \sin\phi\dot{D}_{out\_y\_3}$$

A.2.3 Bearings on shafts

$$\dot{q}_{c_{2\_1}} = \dot{D}_{in\_x\_1}, \quad \dot{q}_{c_{2\_2}} = \dot{D}_{in\_y\_1}, \quad \dot{q}_{c_{3\_1}} = \dot{D}_{in\_x\_9}, \quad \dot{q}_{c_{3\_2}} = \dot{D}_{in\_y\_9}$$

$$\dot{q}_{c_{5\_1}} = \dot{D}_{lay\_x\_1}, \quad \dot{q}_{c_{5\_2}} = \dot{D}_{lay\_y\_1}, \quad \dot{q}_{c_{6\_1}} = \dot{D}_{lay\_x\_9}, \quad \dot{q}_{c_{6\_2}} = \dot{D}_{lay\_y\_9}$$

$$\dot{q}_{c_{7\_1}} = \dot{D}_{out\_x\_1}, \quad \dot{q}_{c_{7\_2}} = \dot{D}_{out\_y\_1}, \quad \dot{q}_{c_{8\_1}} = \dot{D}_{out\_x\_9}, \quad \dot{q}_{c_{8\_2}} = \dot{D}_{out\_y\_9}$$

A.2.4 Gearbox housing

$$\dot{q}_{C_1} = S_f - \frac{1}{I_1}h_{I_1}$$

$$\dot{h}_{I_1} = \frac{1}{C_1}q_{C_1} - \left(R_2\omega_{g_1} + (MTF_1)_{g_1}F_{g_1}^{out1} + (MTF_2)_{g_1}F_{g_1}^{out2} + \frac{(TF_1)_{g_1}}{C_{g_1\_c_1}}q_{g_1\_c_1} + \frac{(TF_2)_{g_1}}{C_{g_1\_c_4}}q_{g_1\_c_4}\right)$$

$$\omega_{g_1} = \dot{\theta}_{g_1} = \frac{1}{I_1}h_{I_1} + \frac{1}{I_5}h_{I_5}$$

$$F_{g_1}^{out1} = \mu N_{g_1}^{out1}\left(\frac{2}{\pi}\right)\arctan\left((v_{g_1}^{out1})(SP)\right) = (F_{11})q_{g_1\_c_2}$$

$$N_{g_1}^{out1} = \frac{(out_1)_{g_1}}{C_{g_1\_c_2}}q_{g_1\_c_2}$$

$$v_{g_1}^{out1} = (MTF_1)_{g_1}\left(\frac{1}{I_1}h_{I_1} + \frac{1}{I_5}h_{I_5}\right) - \frac{1}{(MTF_3)_{g_1}}\left(\frac{1}{I_2}h_{I_2} - \frac{1}{I_5}h_{I_5}\right)$$

$$SP = 100\,(Slope\,Parameter),$$

$$\mu = Friction\;Coefficient\,(0.005)$$

$$F_{g_1}^{out2} = \mu N_{g_1}^{out2}\left(\frac{2}{\pi}\right)\arctan\left((v_{g_1}^{out2})(SP)\right) = (F_{12})q_{g_1\_c_5}$$

$$N_{g_1}^{out2} = \frac{(out_2)_{g_1}}{C_{g_1\_c_5}}q_{g_1\_c_5}$$

$$v_{g_1}^{out2} = (MTF_2)_{g_1}\left(\frac{1}{I_1}h_{I_1} + \frac{1}{I_5}h_{I_5}\right) - \frac{1}{(MTF_4)_{g_1}}\left(\frac{1}{I_2}h_{I_2} - \frac{1}{I_5}h_{I_5}\right)$$

$$\dot{h}_{I_2} = -\frac{1}{C_4}q_{C_4} - R_3\omega'_{g_1} + \frac{F_{g_1}^{out1}}{(MTF_3)_{g_1}} + \frac{F_{g_1}^{out2}}{(MTF_4)_{g_1}} + \frac{q_{g_1\_c_3}}{(TF_3)_{g_1}C_{g_1\_c_3}} + \frac{q_{g_1\_c_6}}{(TF_4)_{g_1}C_{g_1\_c_6}}$$

$$\omega'_{g_1} = \frac{1}{I_2}h_{I_2} - \frac{1}{I_5}h_{I_5}$$

$$\dot{q}_{C_4} = \frac{1}{I_2}h_{I_2} - \frac{1}{I_3}h_{I_3}$$

$$\dot{h}_{I_3} = \frac{1}{C_4}q_{C_4} - R_4\left(\frac{1}{I_3}h_{I_3} - \frac{1}{I_5}h_{I_5}\right) - \left((MTF_1)_{g_2}F_{g_2}^{out1} + (MTF_2)_{g_2}F_{g_2}^{out2} + \frac{(TF_1)_{g_2}}{C_{g_2\_c_1}}q_{g_2\_c_1} + \frac{(TF_2)_{g_2}}{C_{g_2\_c_4}}q_{g_2\_c_4}\right)$$

$$F_{g_2}^{out1} = \mu N_{g_2}^{out1}\left(\frac{2}{\pi}\right)\arctan\left((v_{g_2}^{out1})(SP)\right) = (F_{21})q_{g_2\_c_2}$$

$$N_{g_2}^{out1} = \frac{(out_1)_{g_2}}{C_{g_2\_c_2}}q_{g_2\_c_2}$$

$$v_{g_2}^{out1} = (MTF_1)_{g_2}\left(\frac{1}{I_3}h_{I_3} - \frac{1}{I_5}h_{I_5}\right) - \frac{1}{(MTF_3)_{g_2}}\left(\frac{1}{I_4}h_{I_4} + \frac{1}{I_5}h_{I_5}\right)$$

$$F_{g_2}^{out2} = \mu N_{g_2}^{out2}\left(\frac{2}{\pi}\right)\arctan\left((v_{g_2}^{out2})(SP)\right) = (F_{22})q_{g_2\_c_5}$$

$$N_{g_2}^{out2} = \frac{(out_2)_{g_2}}{C_{g_2\_c_5}}q_{g_2\_c_5}$$

$$v_{g_2}^{out2} = (MTF_2)_{g_2}\left(\frac{1}{I_1}h_{I_1} + \frac{1}{I_5}h_{I_5}\right) - \frac{1}{(MTF_4)_{g_2}}\left(\frac{1}{I_2}h_{I_2} - \frac{1}{I_5}h_{I_5}\right)$$

$$\dot{h}_{I_4} = -\frac{1}{C_9}q_{C_9} - R_5\left(\frac{1}{I_4}h_{I_4} + \frac{1}{I_5}h_{I_5}\right) + \left(\frac{F_{g_2}^{out1}}{(MTF_3)_{g_2}} + \frac{F_{g_2}^{out2}}{(MTF_4)_{g_2}} + \frac{q_{g_2\_c_3}}{(TF_7)_{g_2}C_{g_2\_c_3}} + \frac{q_{g_2\_c_6}}{(TF_8)_{g_2}C_{g_2\_c_6}}\right)$$

$$\dot{q}_{C_9} = \frac{1}{I_4}h_{I_4} - \frac{1}{R_6C_9}q_{C_9}$$

$$\dot{q}_{C_{10}} = \frac{1}{I_5}h_{I_5}$$

$$\dot{h}_{I_4} = \frac{R_3}{I_2} + \frac{R_4}{I_3} - \frac{R_5}{I_4} - \frac{R_2}{I_1}h_{I_1} - \frac{1}{C_{10}}q_{C_{10}} - \frac{1}{I_5}\left(R_2 + R_3 + R_4 + R_5 + R_7\right)h_{I_5}$$
$$- \frac{(TF_1)_{g_1}}{C_{g_1\_c_1}}q_{g_1\_c_1} - \left((MTF_1)_{g_1}(F_{11}) + \frac{(F_{11})}{(MTF_3)_{g_1}}\right)q_{g_1\_c_2} - \frac{(TF_2)_{g_1}}{C_{g_1\_c_4}}q_{g_1\_c_4}$$
$$- \frac{q_{g_1\_c_3}}{(TF_3)_{g_1}C_{g_1\_c_3}} - \left((MTF_2)_{g_1}(F_{12}) + \frac{(F_{12})}{(MTF_4)_{g_1}}\right)q_{g_1\_c_5} - \frac{q_{g_1\_c_6}}{(TF_4)_{g_1}C_{g_1\_c_6}}$$
$$- \frac{(TF_1)_{g_2}}{C_{g_2\_c_1}}q_{g_2\_c_1} - \left((MTF_1)_{g_2}(F_{21}) + \frac{(F_{21})}{(MTF_3)_{g_2}}\right)q_{g_2\_c_2} - \frac{(TF_2)_{g_2}}{C_{g_2\_c_4}}q_{g_2\_c_4}$$
$$- \frac{q_{g_2\_c_3}}{(TF_3)_{g_2}C_{g_2\_c_3}} - \left((MTF_2)_{g_2}(F_{12}) + \frac{(F_{12})}{(MTF_4)_{g_1}}\right)q_{g_2\_c_5} - \frac{q_{g_2\_c_6}}{(TF_4)_{g_2}C_{g_2\_c_6}}$$

Appendix B: Newmark-β method

This section explains the Newmark-β method [Weaver and Johnston (1987)] to simulate dynamics of finite element shaft bending. For a general many degree of freedom system, the damped equation model is

$$M\ddot{D} + B\dot{D} + KD = A(t) \tag{B.1}$$

where M is the mass matrix, B is the damping matrix, K is the stiffness matrix, $A(t)$ is an external force vector, and D is the displacement vector.

At time t_j, equation (B.1) can be represented as

$$M\ddot{D}_j + B\dot{D}_j + KD_j = A_j \tag{B.2}$$

Similarly, at the next time $t_{j+1} = t_j + \Delta t_j$, equation (B.2) becomes

$$M(\ddot{D}_j + \Delta\ddot{D}_j) + B(\dot{D}_j + \Delta\dot{D}_j) + K(D_j + \Delta D_j) = A_j + \Delta A_j \tag{B.3}$$

Subtraction of equation (B.2) from equation (B.3) produces the incremental equation of motion as

$$M\Delta\ddot{D}_j + B\Delta\dot{D}_j + K\Delta D_j = \Delta A_j \tag{B.4}$$

where, $\Delta\ddot{D}_j$, $\Delta\dot{D}_j$, and ΔD_j are the incremental acceleration, velocity, and displacement vectors, respectively; ΔA_j is the increment in load between times t_j and t_{j+1}.

To numerically solve these equations, Newmark approximated the velocity and displacement of a single degree of freedom system at time t_{j+1}, as follows.

$$\dot{u}_{j+1} = \dot{u}_j + [(1-\gamma)\ \ddot{u}_j + \gamma\ddot{u}_{j+1}]\,\Delta t_j \tag{B.5}$$

$$u_{j+1} = u_j + \dot{u}_j\Delta t_j + [(1/2-\beta)\ \ddot{u}_j + \beta\,\ddot{u}_{j+1}]\,(\Delta t_j)^2 \tag{B.6}$$

where Δt_j is the time step, and β and γ are numerical parameters chosen by the user to expedite stability and speed. The parameter β is generally between 0 and 1/4, and γ is often 1/2.

When we consider a many degree of freedom structure and cast the Newmark-β method into matrix form, equations (B.5) and (B.6) can be written in the incremental matrix form.

$$\Delta\dot{D}_j = [(1-\gamma)\ddot{D}_j + \gamma\ddot{D}_{j+1}]\Delta t_j = \ddot{D}_j\Delta t_j + \gamma\Delta\ddot{D}_j\Delta t_j \tag{B.7}$$

$$\begin{aligned}\Delta D_j &= \dot{D}_j\Delta t_j + \left[\left(\tfrac{1}{2}-\beta\right)\ddot{D}_j + \beta\ddot{D}_{j+1}\right](\Delta t_j)^2 \\ &= \dot{D}_j\Delta t_j + \tfrac{1}{2}\ddot{D}_j(\Delta t_j)^2 + \beta\Delta\ddot{D}_j(\Delta t_j)^2\end{aligned} \tag{B.8}$$

Solving for $\Delta\ddot{D}_j$ and $\Delta\dot{D}_j$, we get

$$\Delta\ddot{D}_j = \frac{1}{\beta(\Delta t_j)^2}\Delta D_j - \hat{Q}_j \tag{B.9}$$

$$\Delta\dot{D}_j = \frac{\gamma}{\beta\Delta t_j}\Delta D_j - \hat{R}_j \tag{B.10}$$

where,

$$\hat{Q}_j = \frac{1}{\beta\Delta t_j}\dot{D}_j + \frac{1}{2\beta}\ddot{D}_j \tag{B.11}$$

$$\hat{R}_j = \frac{\gamma}{\beta}\dot{D}_j + \left(\frac{\gamma}{2\beta} - 1\right)\Delta t_j\ddot{D}_j \tag{B.12}$$

If we substitute equations (B.9) and (B.10) into the incremental equations of motion (B.4), then we have

$$\hat{K}\Delta D_j = \Delta\hat{A}_j \tag{B.13}$$

where,

$$\hat{K} = K + \frac{1}{\beta(\Delta t_j)^2}M + \frac{\gamma}{\beta\Delta t_j}C \tag{B.14}$$

$$\Delta\hat{A}_j = \Delta A_j + M\hat{Q}_j + C\hat{R}_j \tag{B.15}$$

From equations (B.13), the unknown incremental displacements ΔD_j are obtained. Finally, the values of D_j, $\dot{D}_j$, and $\ddot{D}_j$ at the next time t_{j+1} are

$$D_{j+1} = D_j + \Delta D_j \tag{B.16}$$

$$\dot{D}_{j+1} = \dot{D}_j + \Delta\dot{D}_j \tag{B.17}$$

$$\ddot{D}_{j+1} = \ddot{D}_j + \Delta\ddot{D}_j \tag{B.18}$$

Appendix C: Nomenclature

β, γ	Parameters of Newmark's method
ϕ	Pressure angle
ρ	density
μ	friction coefficient
$A(t)$, A	external force vector in Newmark's method
a	input force vector to a finite element part

B	damping matrix in Newmark method, state pace matrix
D	displacement vector
ΔD, ΔA	incremental displacement vector and increment in load
F	input source vector applied to a bond graph part
F_n, F_t	normal and tangential forces at contact surface of gear teeth
$\underline{f}, \underline{p}$	vector of flows and momentum variables
M, K	mass and stiffness matrices in Newmark's method
$[m]$, $[k]$	mass and stiffness matrices of an element
$[M]_i$, $[K]_i$	extended mass and stiffness matrices of elements
P	matrix which relates a bond graph part to a finite element part
Q	matrix which relates a finite element part to a bond graph part
u	displacement of single degree of freedom
v_n, v_t	normal and tangential velocities at contact surface of gear teeth
$\{W\}_i$	extended nodal displacement vector of elements
$\{w\}_i$	nodal displacement vector of an element
X	state vector of a bond graph part
$\theta_{g_1}, \theta_{g_2}$	rotational angles in gear contact sub-models, g_1 and g_2
h_{I_5}	angular momentum of gearbox housing in gearbox model
h_{I_1}, h_{I_2}, h_{I_3}, h_{I_4}	angular momenta of shafts in gearbox model
$P_{g_1\_i_1}, P_{g_1\_i_2}$, $P_{g_1\_i_3}, P_{g_1\_i_4}$, $P_{g_2\_i_1}, P_{g_2\_i_2}$, $P_{g_2\_i_3}, P_{g_2\_i_4}$	momenta of gear teeth by gear tooth inertia in contact sub-models, g_1 and g_2
$q_{g_1\_c_1}, q_{g_1\_c_2}$, $q_{g_1\_c_3}, q_{g_1\_c_4}$, $q_{g_2\_c_1}, q_{g_2\_c_2}$, $q_{g_2\_c_3}, q_{g_2\_c_4}$	bending deflections of gear teeth in contact sub-models, g_1 and g_2
$q_{g_1\_c_5}, q_{g_1\_c_6}$, $q_{g_2\_c_5}, q_{g_2\_c_6}$	deformations of gear teeth flank by contact in contact sub-models, g_1 and g_2.
$q_{c_{2\_1}}, q_{c_{2\_2}}$, $q_{c_{3\_1}}, q_{c_{3\_2}}$, $q_{c_{5\_1}}, q_{c_{5\_2}}$, $q_{c_{6\_1}}, q_{c_{6\_2}}$, $q_{c_{7\_1}}, q_{c_{7\_2}}$, $q_{c_{8\_1}}, q_{c_{8\_2}}$	deflections of bearings at both ends of shaft in finite element shaft sub-model
$q_{C_1}, q_{C_4}, q_{C_9}$	angular displacements of each shaft by torsion in gearbox model
$q_{C_{10}}$	angular displacement of gearbox housing in gearbox model